Dielectrophoretic Manipulation of Particles and Lymphocytes Using Rail-type Electrodes

Kazuya TATSUMI [1,2,*], Haruka OKUI[1], Koki KAWANO[1], Kazuyoshi NAKABE[1,2]

* Corresponding author: Tel.: ++81 (75)383 3606; Fax: ++81 (75)383 3608;
Email: tatsumi@me.kyoto-u.ac.jp
1 Department of Mechanical Engineering and Science, Kyoto University, JAPAN
2 Advanced Research Institute of Fluid Science and Engineering, Kyoto University, JAPAN

Abstract A particle manipulation and sorting device using the dielectrophoretic (DEP) force is described in this study. The device consists of "ladder-type", "flip-type" and "oblique rail-type" electrode regions. The ladder-type and rail-type electrodes can generate a DEP force distribution that captures the particles, the DEP force of which is "negative" (repulsion force), in the area located at the center of the electrodes. The particles can then be guided individually along the electrode. In addition to this, the ladder-type electrode can align the particles with equal spacing in the streamwise direction. Using the "flip-type" electrode, which pushes the particles away, in combination with these electrodes, the direction of the particle can be selected with high accuracy, reliability and response. In the first half of this paper, numerical simulation was carried out to calculate the particle motion and evaluate the performance of the ladder-type electrode. Several models were validated to investigate the influences of the non-uniformity of the electric field and the electric interaction of the surface charges and polarizations. Measurement using the high-speed camera was then carried out to investigate the motions of the particles and sorting reliability. The trajectories and the probability density functions of the particles at the inlet and outlet of the electrode region showed that by using these electrodes the particles can be aligned, sorted and guided accurately.

Keywords: Micro Flow, Dielectrophoretic Force, Sorting, Manipulation, Micro-particles and Cells

1. Introduction

The technologies for manipulating and sorting cells and microparticles in the microchannel flow have been studied intensively in the last decade. Those using DEP force has been one of the promising tools because it can produce a driving force to the particles or cells without changing or modifying them or the fluid properties (Chen et al. 2008, Gagnon 2011, Yi et al. 2006, Zhang et al. 2010). Although many types of electrodes and channels have been proposed in other studies, substantial issues remain to be solved for satisfying the demands of the applications, such as accuracy, sorting rate, response and applicability under various conditions. One such problem is because the DEP force, F_{DEP}, is mainly produced by the electric field gradient, it decays markedly with the distance from the electrode. Other problems are the fact that in many cases, a

(a) schematic of the microchannel and electrodes

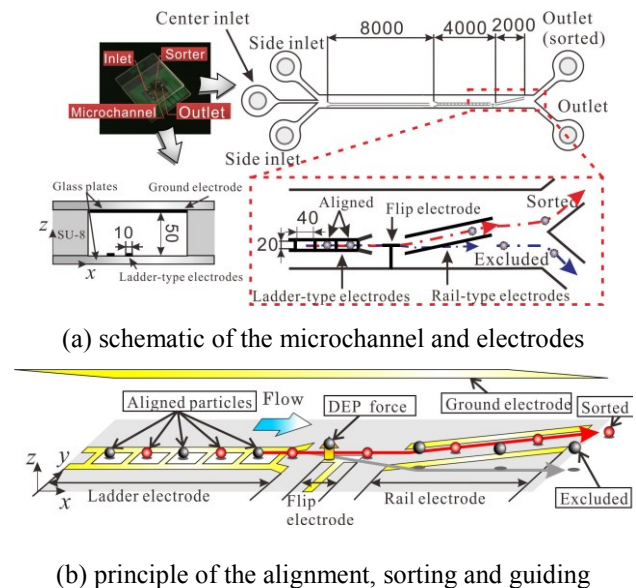(b) principle of the alignment, sorting and guiding

Fig. 1: (a) Schematics of the microchannel and electrodes in the present micro-device, and (b) the schematic showing the concept of the alignment and sorting, and particle motions in the present device.

negative F_{DEP}, namely a repulsion force

against the electrode works on the particle or cell, and that the distance between the particles flowing in the channel are random and not aligned. It is, therefore, difficult to precisely control the particle position. In order to overcome these problems, an electrode patterns, which are not only effective but also fundamental and versatile, is developed in this study.

The Schematic of the electrode patterns are shown in Fig. 1. The manipulation and sorting device consists of the ladder-type electrode, the flip-type electrode and the oblique rail-type electrode regions (Tatsumi et al. 2013). These electrodes are attached to the channel bottom wall, and the top wall is an electrode connected to the ground. The ladder-type will produce F_{DEP} which work on the particles to make them align not only at the centerline but also in equal spacing. The flip-type operating as a gate electrode will lift the particle when necessary and exclude it from the electrode region. The remaining particles will be guided along the oblique rail-type electrodes and can be collected.

2. Methods

2.1 Numerical methods

To calculate the dielectrophoretic force, Calusius-Mossotti (CM) function (Cetin and Li 2011), Multipole (Washizu ad Jones 1994, Jones and Washizu 1996), and Force density methods were first applied and evaluated in order to validate the numerical scheme applied to the present computation. The means of computation using the CM function can be defined as Eq. (1).

$$F_{DEP} = 2\pi\varepsilon_0\varepsilon_1' R^3 \, \mathrm{Re}[\underline{K}_{CM}]\nabla E_{rms}^2 \qquad (1)$$

$$\underline{K}_{CM} = \frac{\underline{\varepsilon_2} - \underline{\varepsilon_1}}{\underline{\varepsilon_2} + 2\underline{\varepsilon_1}}, \quad \underline{\varepsilon} = \varepsilon_0\varepsilon' + \frac{\kappa}{i2\pi f}$$

where, ε_0 is the dielectric constant of vacuum, ε' is the relative dielectric constant, $\underline{\varepsilon}$ is the complex dielectric constant, and κ is the electric conductivity. f is the frequency of the alternate current, K_{CM} is the CM function. The underline indicates the complex value, and the subscripts shows the values of fluid and solid.

Since the lymphocyte has a shell structure, the layers with different properties of the cell

Table 1: Physical properties of the nucleated cell.

R_{nc}[μm]	d_{ne}[μm]	R_{cell}[μm]	d_{cm}[μm]
4.9	0.04	6	0.007
ε'_{np}	κ_{np}[1/Ω·m]	ε'_{ne}	κ_{ne}[1/Ω·m]
52	1.35	28	6×10^{-3}
ε'_{cp}	κ_{cp}[1/Ω·m]	ε'_{cm}	κ_{cm}[1/Ω·m]
60	0.32	6.8	1×10^{-3}

Table 2: Physical properties of PBS and PS particle.

ε'_{PBS}	κ_{PBS}[1/Ω·m]	ε'_{PS}	κ_{PS}[1/Ω·m]
78.3	1.55	2.65	0

membrane, cytoplasm, nuclear envelope, and nucleoplasm are simplified on the basis of the of model presented by Asami et al (1989) and Hanai et al (1992).

The model using the CM function applies the 1st order approximation for the external electric field. However, the electric potential in the microchannel shows a strong non-uniformity, and the electric potential may not be calculated correctly under this approximation. Therefore, the second model employed in the present study is the one considering the multi-pole. The F_{DEP} in this case can be written as Eq. (3).

$$F_{DEP} = \sum F^{(n)} \qquad (3)$$

$$F^{(n)} = \frac{2\pi\varepsilon_0\varepsilon_1' R^3}{(n-1)!(2n-1)!!} \mathrm{Re}[\underline{K}n^{(n)}]\nabla\left\{\left((\nabla)^{n-1} E_0\right)_{rms}\right\}^2$$

$$\underline{K}^{(n)} = \frac{\underline{\varepsilon_2} - \underline{\varepsilon_1}}{(n+1)\underline{\varepsilon_1} + n\underline{\varepsilon_2}}$$

$$\left((\nabla)^{n-1} E_0\right)_{rms} = \sqrt{\frac{1}{2}\left\{(\nabla)^n \underline{E}_0 (\nabla)^n \underline{E}_0^*\right\}}$$

When calculating the multi-layer structure of the lymphocyte, the following equation defining the equivalent complex relative dielectric constant is applied to calculate $K^{(n)}$.

$$\left(\underline{\varepsilon}_{2,eq}\right)_n = \underline{\varepsilon}_2 \frac{a^{2n+1} + (n+1)\underline{K}^{(n)}}{a^{2n+1} - n\underline{K}^{(n)}} \qquad (4)$$

The third model is the force density method. Time mean value of the F_{DEP} of a particle with arbitrary shape can be calculated using the following equation.

$$F_{DEP} = \frac{1}{2}\left[\int_{all}\left[\rho_{free}\underline{E}_0^* + (\underline{P}_{eff}\cdot\nabla)\underline{E}_0^*\right]dV\right] \quad (6)$$

$$\underline{P}_{eff}(r) = (\varepsilon(r) - \varepsilon_1)\underline{E}_{ind}$$

ρ_{free} is the density of the free charge, $\underline{P}_{eff}$ is the effective polarization. $\underline{E}_0$ is the external electric field, and $\underline{E}_{ind}$ is the electric field induced by the presence of the particle. F_{DEP} calculated by each model are referred to as F_{CM}, F_{MP} and F_{FD}.

The electric field was calculated using the COMSOL multyphysics ver. 4.3a by solving the Poisson equation. In the case of F_{FD}, not only the external electric field but also the electric field considering the electric interaction between the fluid and particle or lymphocyte parts. We will need to calculate the electric field in the areas of cell membrane, cytoplasm, nuclear envelope, and nucleoplasm. Since the thickness of the cell membrane and nuclear envelope are significantly small, directly generating mesh in this area requires serious computational cost. Therefore, the boundary condition shown by Eq. (7) is applied to each boundary in the present study. This model calculates the potential drop at the layer of the membrane directly and reduce the computational cost.

$$\underline{J}\cdot n = \frac{(\kappa_{mem} + i2\pi f\varepsilon_0\varepsilon_{mem}')(V_{out} - V_{in})}{t_{mem}} \quad (7)$$

J is the current density, **n** is the normal vector of surface. V_{out} and V_{in} are the potential at the inner and outer side of the boundary. ε_{mem}', κ_{mem} and t_{mem} the relative dielectric constant of the membrane, conductivity, and membrane thickness. The properties applied to the cell in the computation are summarized in Table 1 reffering the results of Asami et al. (1989). These are the values for lymphocyte of a mouse. The radius of the nucleus was obtained on the basis of the ratio of the nucleus and cell radii, which the value 55% is used in this study (Shmid-Schonbein, 1990). Subscripts cm, cp, ne, and np presents the values of cell membrane, cytoplasm, nuclear envelope, and nucleoplasm, respectively. The diameters of the particle and cell are 6μm. The properties of the fluid and polystyrene particle are shown in

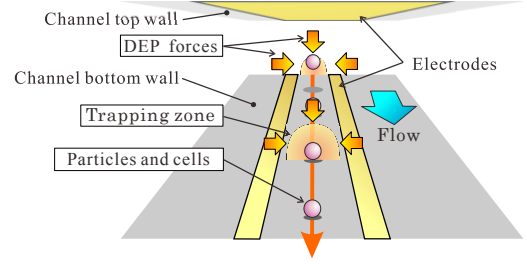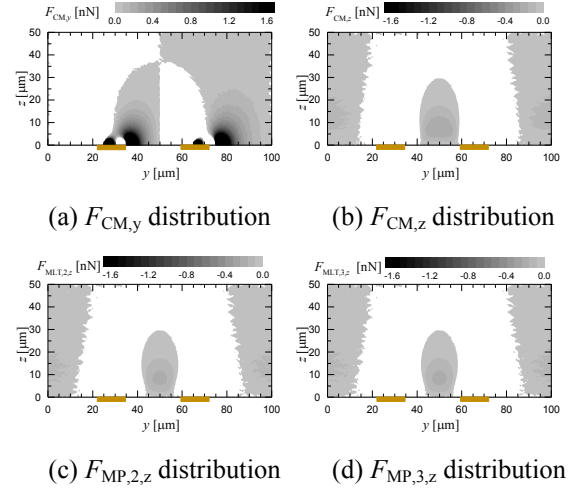Fig. 2: Schematics of motion of the particle trapped and guided by the rail-type electrodes.

(a) $F_{CM,y}$ distribution   (b) $F_{CM,z}$ distribution

(c) $F_{MP,2,z}$ distribution   (d) $F_{MP,3,z}$ distribution

Fig. 3: The distributions of the DEP forces F_{CM} and F_{MP} working on the Jurkat cell in the case of rail-type electrode at the cross-sectional plane. $F_{MP,2}$ and $F_{MP,3}$ present the force of the multi-pole model considering 2nd and 3rd order term, respectively.
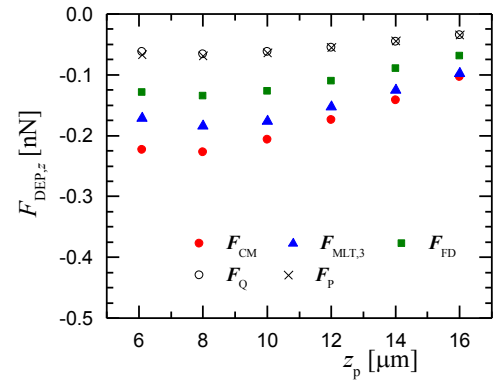

Fig. 4: The influence of the z positions on the DEP force working on the Jurkat cell. Comparison is made among computation applying the three models.

Table 2.

2.2 Experimental methods

Micro-device was fabricated using top and bottom walls made of glass substrates with Pt electrode pattern bonded with SU-8 (Micro
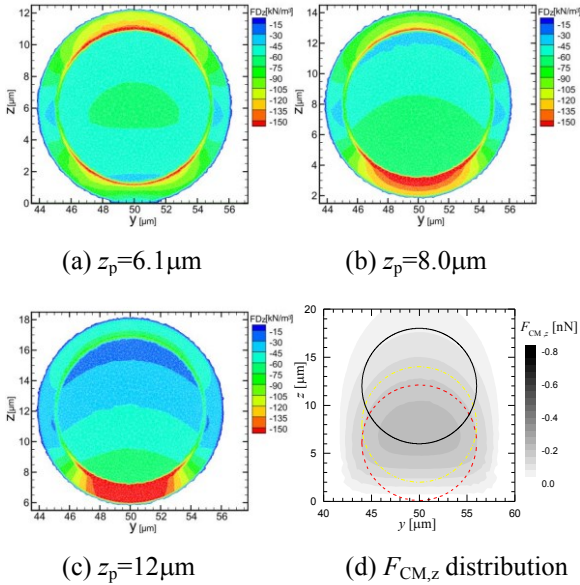
(a) z_p=6.1μm   (b) z_p=8.0μm

(c) z_p=12μm   (d) $F_{CM,z}$ distribution

Fig. 5: (a)–(c) Distributions of the force density of the Jurkat cell located at different z positions using the force density model, and (d) the distributions of $F_{CM,z}$. The circles shown in (d) displays the surfaces of the cell at different heights.

Chem Co.). The microchannel shown in Fig. 1 (a) was patterned in the SU-8 layer. The channel width and height are 200 and 50 μm, respectively.

Sheath flow was supplied from the upstream using three inlet flows. The particles and lymphocytes were supplied from the center inlet, and the spanwise position was roughly controlled.

Two electrode patterns were employed in the experiment. One is the combination of rail-type, ladder-type and flip-type electrodes illustrated in Fig. 1. The present ladder-type electrode is able to trap and guide the particles at certain height and spanwise positions, and moreover, with even streamwise spacing of each particle. The flip-electrode will push the particles in the height direction and exclude them when the voltage is supplied to the electrode and activated. The rail-type electrode located downstream will trap the particles passing the flip-type electrode (when not activated), guide them in the spanwise direction, and can be collected from another reservoir located downstream. Detail explanation on the function of the ladder-type electrode will be discussed shortly.
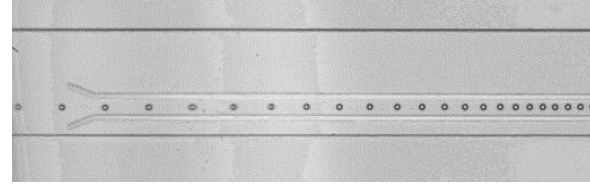
The other electrode is the simple rail-type

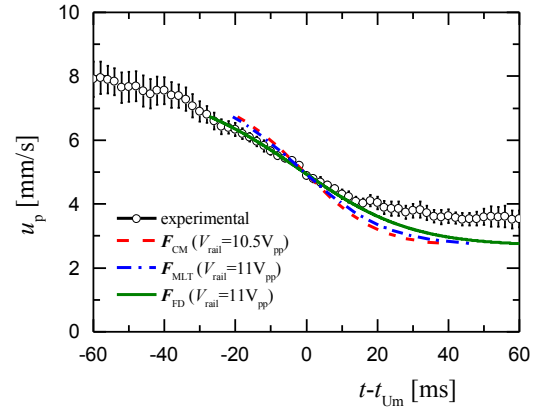Fig. 6: Composite stroboscopic photo of the particle in the case of V_{p-p}=20V and U_m=4.94mm/s.

Fig. 7: Relationship between u_p and t of experiment, and computation using F_{CM}, F_{MP} and F_{FD}.

electrode shown in Fig. 2. This electrode is used to verify the model and numerical scheme of the present computation.

Peak to peak voltage of 20V was supplied to the rail-type electrode at the frequency of 10MHz. In the case of ladder-type electrode, the voltage of 10MHz to generate DEP force was additionally oscillated with periods of low frequency in order to align the particles in the streamwise direction.

Polystyrene (PS) particles of nominal diameter 6μm (Thermofisher scientific, 4112A) were used as micro-particles. Jurkat cells (ATCC: CRL2570) were used as lymphocytes. These were suspended in phosphate buffered saline (PBS). In the case of PS particles, sodium lauryl sulfate was added to the solution with 0.1wt% to prevent the particle attach to the channel wall.

3. Results and Discussion
3.1 Numerical verification
Particle were supplied to the rail-type electrode with the flow rate of Q =3.2μL/min and U_m=4.94mm/s. The particle motion was recorded by a high-speed video camera and the

position and velocity of the particle was measured.

Figures 3 (a) and (b) show the distributions of the y and z components of the F_{CM} on the y–z plane. (c) and (d) show the z component of F_{DEP} in the case of MP model. (c) and (d) shows the results when the 2nd and 3rd order terms are considered, respectively.

F_{DEP} generated by the rail-type electrode moves the particles toward the channel centerline and close to the bottom wall. By this, the particle position can be controlled, and allows us to guide the particle in the channel with high accuracy.

The minimum value of F_{CM} is $F_{CM,z} = -0.42$nN in Fig. (b). However, in the case of $F_{MP,2}$ shown in (c), the value is -0.4nN and is larger than that of F_{CM}. The 1st order term $F_z^{(1)}$ is proportional to the z gradient of E_{rms}^2. $F_z^{(2)}$ is proportional to the z gradient of $\nabla E : \nabla E^*$. These values are positive and negative in the area adjacent to the channel bottom wall. Thus, $F_{MP,2}$ slightly increases compared with F_{CM}. The third term showing the influence of $\nabla\nabla E_{rms}$ appears to be small in the rail-type electrode case.

Figure 4 shows the F_{DEP} distribution against the height position in the case of Jurkat cell. The Coulomb force working on the membrane surface F_Q and the force related to the polarization F_P, both composing the F_{FD}, are shown in the figure. In Fig. 5, the distributions of the force density at different z locations are shown. For comparison, the F_{CM} distribution is shown in Fig. (d).

In Fig. 4, the values of F_Q and F_P are nearly equal. Although not shown here, in the case of PS particles, F_P was dominant and F_Q was nearly zero due to the fact that PS particle could be considered as a conductive body. On the other hand, in the lymphocyte case, the charges on the membrane and nuclear envelope increases, and the influence of the Coulomb force becomes noticeable.

In Fig. 5, the distribution of F_{FD} and F_{CM} shows similar value in the nucleoplasm. The distribution in the area of nucleoplasm shows similar trend. On the other hand, in cytoplasm a large difference can be observed where F_{FD} of large value is observed in the z axis. In the
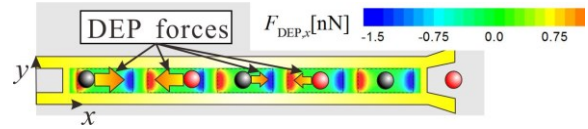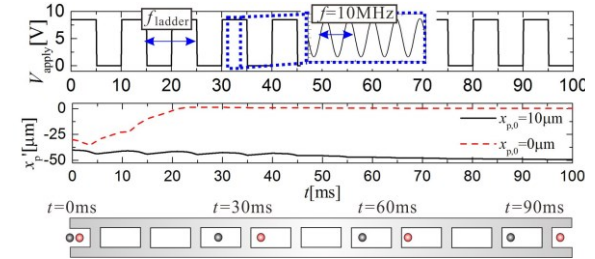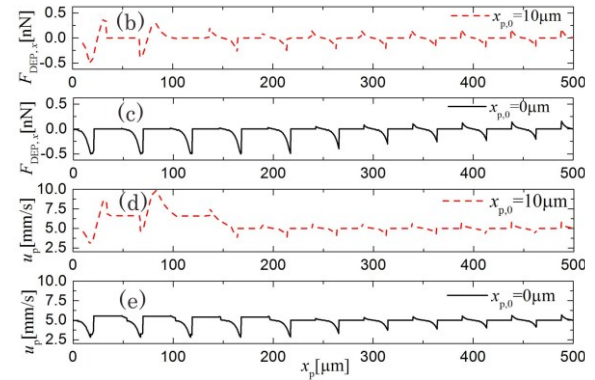

Fig. 8: DEP force working on the particle for alignment

(a) relative positions of the particles converging to certain positions with equally spaced

(b)~(e) The streamwise components of F_{DEP} and the streamwise velocity of the particle u_p in relation to the streamwise position x_p.

Fig. 9: (a) The relative positions of the particles initially located at $x_{p,0}=0$ and $10\mu m$ at $t=0$s and the applied low frequency oscillation, and (b) & (c) the F_{DEP} applied to the particles in these two cases, and (d) & (e) their streamwise velocities (particle velocity=11.6mm/s).

case of nucleoplasm, the influence of the non-uniformity of the electric field is dominant, and at the cytoplasm, effect of the interaction of the polarization and charges additionally becomes noticeable.

As for the influence of the height position z_p, one can see in Fig. 4 that F_{CM}, $F_{MLT,3}$ and F_{FD}, differs equally at z_p showing that the influences of the electric field non-uniformity and electric interaction exist similarly. However, as z_p increases, F_{CM} approaches to $F_{MLT,3}$ indicating that the effect of the non-uniformity decreases as the lymphocyte distance itself from the electrode. However,
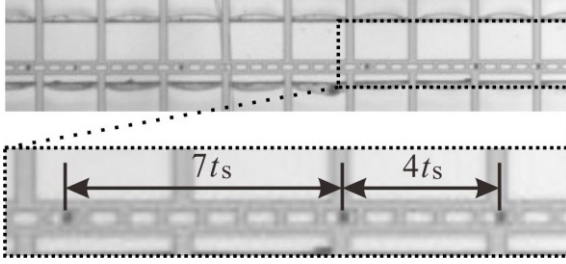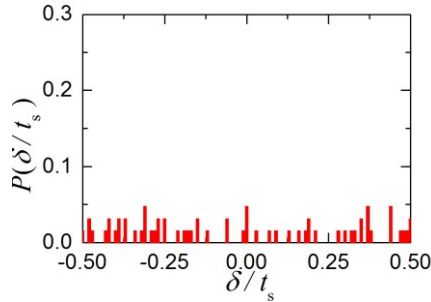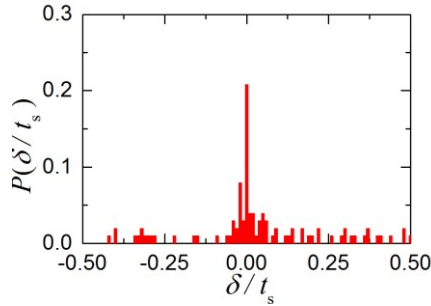
Fig. 10: Snapshots of the particles aligned equally spaced as they flow along the ladder-type electrodes.

(a) f_{ladder} oscillation non-activated

(b) activated

Fig. 11: Probability density distributions of the deviation of the particles δ from the synchronized time of the oscillation (Measured at the outlet of the ladder-type electrodes).

the interaction effect still exists strongly even at z_p=15 showing that we need to employ the fluid density model in order to calculate the F_{DEP} correctly in the case of nuclear cell.

Figure 6 shows the snapshots of a particle flowing above the rail-type electrodes. The photograph is a superposition of images recorded with an interval of 5ms. One can see that the distance between the particles decreases and converges to a constant value as the particle flow downstream. This indicates that the particle is trapped by the F_{DEP} and moves toward the channel bottom wall, and eventually flow with a constant velocity.

Figure 7 compares the numerical and

experimental results. The figure shows the distribution of the particle streamwise velocity u_p. The abscissa axis presents the time, and t_{Um} is the period when the cell reaches the bottom wall and the velocity becomes constant. The error bars shows the 95% uncertainty on the basis of the ASME standard.

Comparing the three models, the results using the fluid density model agrees well the experimental data. The results of the CM function and the multi-pole model, on the other hand, show deviation by 70% and 20%. This concludes that in the case of microchannel flows, the F_{DEP} calculated using the CM function may not be correct due to the non-uniformity of the electric field, and moreover, to the electric interaction due to the presence of the nucleus.
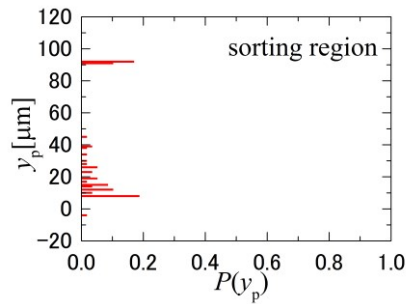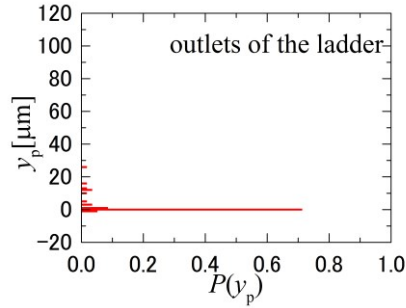
3.2 Numerical evaluation of particle motions for ladder-type electrodes

The numerical model and scheme evaluated in Section 3.1 was used to calculate the particle motions in ladder-type electrode. The ladder-type electrode shown in Fig. 1 consists of two streamwise parallel electrodes and numbers of traverse electrodes. As described in Section 2.2, low-frequency, f_{ladder}, fluctuation of square wave is added to the high frequency fluctuation of 10MHz. When the voltage is applied to the electrode (activated), F_{DEP} the distribution of which is shown in Fig. 8, will work on the particle. This force will work in the direction not only toward the channel bottom wall but also in the streamwise direction if the particle is not located at the streamwise center of the traverse electrodes.
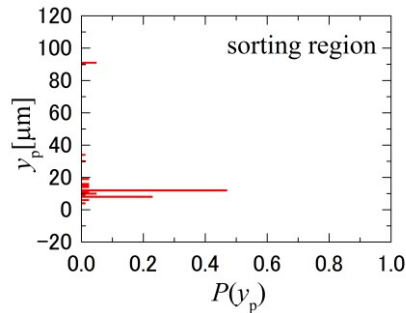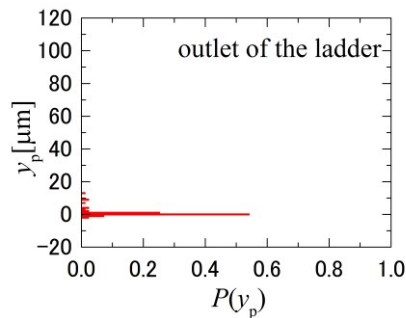
Figure 9 (a) shows the schematic of the applied voltage pattern and the relationship between the relative streamwise position of the particle to the center of the traverse electrodes, x_p', and time, t. Figure 9 (b) shows the streamwise component of F_{DEP} and particle velocity u_p distributions against x_p.

The initial position of the particles are x_p'=0 and 10μm which is the relative position at t=0. The mean flow velocity is 11.6mm/s, and f_{ladder}=100Hz.

The $F_{DEP,x}$ and u_p distributions shown in Fig. 9 indicate that the force is working on the

depending on its initial position.

3.3 Experimental results of the sorting system

Figure 10 shows a photograph of the particle flowing in the ladder-type electrodes. The particles are located at the same position relative to the traverse electrodes. The time interval of each particle measured by the high-speed camera were exactly $7t_s$ and $4t_s$, where t_s is $1/f_{ladder}$ which is the period of the low frequency fluctuation.

Figure 11 shows the probability density distributions of the deviation of the particle from the synchronized time of the low frequency oscillation of the applied voltage. δ is the deviation and is normalized by t_s. (a) is the case when only high frequency voltage is applied to generate the F_{DEP}, and (b) shows the results when the electrode is activated. Both cases were measured at the outlet of the ladder-type electrode. In Fig. (a), P is scattered across the δ/t_s region indicating that the particles flowing from the electrode region are not aligned and randomly distributed. On the other hand, a peak is observed near the region of $\delta/t_s=0$ showing that the particle are aligned to match the period of the low frequency fluctuation.

These results show that by flowing along the ladder electrodes, the particle positions are aligned equally spaced.

Figure 12 shows the probability density distributions of the particle spanwise position at the locations of the outlets of the ladder-type electrode and the sorting region. The flip-electrode shown in Fig. 1 is activated (voltage is applied to the electrode) only at the moment when the particle is expected to flow above the electrode. Namely, the flip-electrode is activated at the timing synchronized with t_s of the ladder-type electrode.

Figure (a) shows the non-activated case and (b) is for the case of activated one. In the cases of (a) and (b), the spanwise position are controlled to be as $y_p=0\mu m$. In Fig. (a), the P of y_p distributes in the range of $0<y_p<40$ and $y_p=90$. The former group is for the particle excluded by the flip-electrode and flowing downstream. The distribution has a broad

(a) F_{DEP} with f_{ladder} oscillation non-activated

(b) F_{DEP} with f_{ladder} oscillation activated

Fig. 12: Probability density distributions of the particle spanwise positions y_p at the outlets of the ladder-type electrodes and the sorting region. All particles are synchronized accurately and flipped when activated.

particle in the positive and negative directions depending on the deviation of position. As the time elapse, $F_{DEP,x}$ converges to zero, and u_p approaches to a velocity which is related to height position of the particle. Therefore, x_p' also converges and remains constant in the downstream region at a relative position

range indicating that at the period when the flip-electrode is activated the relative position of the particle against the electrode varies. This means that even though the particles are excluded there is a mismatch with the timing. The latter group in the distribution depicts those which passed the flip-electrode without any interference, and captured by the oblique rail-type electrodes. This should not occur if the flip-type electrode is operated correctly.

On the other hand, a clear peak is observed at y_p=10μm in Fig. (b). This shows that all the particles are excluded at an exact timing when the low frequency fluctuation at the ladder-type electrode is activated.

These results show that by aligning the particles in the streamwise direction with the ladder-type electrode, the particles can be excluded in a precise timing. This confirms that the particles which are excluded and collected by the oblique-type electrodes can be sorted in high accuracy which leads to enhancing the sorting performance.

4. CONCLUSIONS

Numerical computation and measurements were conducted to evaluate the performance of the micro-device for sorting and manipulation using the ladder-type, flip-type and oblique-rail-type electrodes.

Computations using the CM function, multi-pole model, and fluid density model were carried out. The electric charge on the membrane and nuclear envelope, and the polarization in cytoplasm and nucleus showed a large effect on the F_{DEP} working on the lymphocyte. Comparing the numerical results with the experiment, the fluid density model showed the highest accuracy, while the CM function and multi-pole showed 70% and 20% deviation in the particle velocity distributions.

The simulation showed that the ladder-type electrode can control the particles positions and align them with even spacing in the streamwise direction. Measurement showed that by this particle alignment, the performance of the sorting using the flip-type electrode enhanced markedly. The probability function of the particle position confirmed the accuracy of the present sorting micro-device.

REFERENCES

Chen, P., Feng, X., Du, W., and Liu, B.-F., 2008. Microfluidic Chips for Cell Sorting, Frontiers in Bioscience 13, 2464.

Gagnon, Z. R., 2011. Cellular Dielectrophoresis: Applications to the Characterization, Manipulation, Separation and Patterning of Cells, Electrophoresis 32, 2466.

Tatsumi, K., Shintani, H., Katsumoto, Y., and Nakabe, K., 2013. Dielectrophoretic sorting of microparticles and lymphocytes using rail-type electrodes, micro-TAS2013.

Yi, C., Li, C., Ji, S., and Yang., M, 2006. Microfluidics technology for manipulation and analysis of biological cells, Analytica Chimica Acta 560, .1-23.

Zhang, C., Khoshmanesh, K., Mitchell, A., and Kalantar-Zadeh, K., 2010. Dielectrophoresis for manipulation of micro/nanoparticles in microfluidic systems, Analytical and Bioanalytical Chemistry 396, 401-420.

Cetin, B., and Li, D., 2011. Dielectrophoresis in microfluidics technology, Electrophoresis 32, 2410-2427.

Washizu, M., and Jones, T.B., 1994. Multipolar dielectrophoretic force calculation, Journal of Electrostatics 33, 187-198.

Jones, T.B., and Washizu, M., 1996. Multipolar dielectrophoretic and electrorotation theory, J. of Electrostatics 7, 121-134.

Asami, K., Takahashi, Y., and Takashima, S., 1989. Dielectric properties of mouse lymphocytes and erythrocytes, Biochimica et Biophysica Acta, 49-55.

Hanai, T., 1968. Electric properties of emulsions, in Emulsion Science (Ed.: Sherman, P.) Academic Press, London, 353-478.

Shmid-Schonbein, G.W., 1990. Leukocyte Biophysics, Cell Biophysics, 107-135.